# Defining the Binding Site of Homotetrameric R67 Dihydrofolate Reductase and Correlating Binding Enthalpy with Catalysis†

Michael Brad Strader,‡ Shaileja Chopra,‡ Michael Jackson,‡ R. Derike Smiley,‡ Lori Stinnett,‡ Jun Wu,§ and Elizabeth E. Howell*,‡

*Department of Biochemistry, Cellular and Molecular Biology, University of Tennessee, Knoxville, Tennessee 37996-0840, and Graduate School of Genome Science and Technology, University of Tennessee, Knoxville, Tennessee 37996-0840*

*Received February 17, 2004; Revised Manuscript Received April 21, 2004*

ABSTRACT: R67 dihydrofolate reductase (DHFR) is a novel protein that possesses 222 symmetry. A single active site pore traverses the length of the homotetramer. Although the 222 symmetry implies that four symmetry-related binding sites should exist for each substrate as well as each cofactor, isothermal titration calorimetry (ITC) studies indicate only two molecules bind. Three possible combinations include two dihydrofolate molecules, two NADPH molecules, or one substrate with one cofactor. The latter is the productive ternary complex. To evaluate the roles of A36, Y46, T51, G64, and V66 residues in binding and catalysis, a site-directed mutagenesis approach was employed. One mutation per gene produces four mutations per active site pore, which often result in large cumulative effects. Conservative mutations at these positions either eliminate the ability of the gene to confer trimethoprim resistance or have no effect on catalysis. This result, in conjunction with previous mutagenesis studies on K32, K33, S65, Q67, I68, and Y69 [Strader, M. B., *et al*. (2001) *Biochemistry 40*, 11344−11352; Hicks, S. N., *et al*. (2003) *Biochemistry 42*, 10569−10578; Park, H., *et al*. (1997) *Protein Eng. 10*, 1415−1424], allows mapping of the active site surface. Residues for which conservative mutations have large effects on binding and catalysis include K32, Q67, I68, and Y69. These residues form a stripe that establishes the ligand binding surface. Residues that accommodate conservative mutations that do not greatly affect catalysis include K33, Y46, T51, S65, and V66. Isothermal titration calorimetry studies were also conducted on many of the mutants described above to determine the enthalpy of folate binding to the R67 DHFR·NADPH complex. A linear correlation between this $\Delta H$ value and log $k_{cat}/K_m$ is observed. Since structural tightness appears to be correlated with the exothermicity of the binding interaction, this leads to the hypothesis that enthalpy-driven formation of the ternary complex in these R67 DHFR variants plays a strong role in catalysis. Use of the alternate cofactor, NADH, extends this correlation, indicating preorganization of the ternary complex determines the efficiency of the reaction. This hypothesis is consistent with data suggesting R67 DHFR uses an *endo* transition state (where the nicotinamide ring of cofactor overlaps the more bulky side of the substrate's pteridine ring).

Dihydrofolate reductase (DHFR)[1] catalyzes the NADPH-dependent reduction of 7,8-dihydrofolate to 5,6,7,8-tetrahydrofolate. This reaction plays a crucial role in folate metabolism as tetrahydrofolate plays a vital function as a one-carbon donor in the synthesis of thymidylate, purine nucleosides, and other metabolic intermediates. Inhibition of this enzyme leads to blockage of DNA synthesis and eventually cell death. Trimethoprim (TMP) is an antibacterial drug that inhibits bacterial DHFRs (*4*). Resistance to TMP arises from production of DHFR variants that typically bind more weakly to the drug. Type II R-plasmid-encoded R67 DHFR is of particular interest as it is genetically and structurally unrelated to chromosomal DHFRs (*5*).

R67 DHFR is one of the smallest proteins known to assemble into an active enzyme. Each monomer is 78 amino acids long; however, the first 16 residues can be removed without affecting the $\beta$-sheet structure and thus activity (*6*). The active species is a homotetramer, and the crystal structure describes a toroid with a pore traversing the length of the protein [PDB entry 1VIE (*7*)]. As shown in Figure 1, a hallmark of the structure is its 222 symmetry. Difference Fourier maps describing bound folate indicate the pore is the active site (1VIF). Because of this symmetry, R67 DHFR displays three different ligand binding combinations: two substrates (folate or DHF), two NADPH molecules, or one substrate with one NADPH. The latter is the productive ternary complex. Binding of NADPH displays negative cooperativity ($K_d$ values of 2.5 and 95 $\mu$M), while binding

† This research was supported by NSF Grant MCB-0131394 (to E.E.H.).

* To whom correspondence should be addressed. Phone: (865) 974-4507. Fax: (865) 974-6306. E-mail: lzh@utk.edu.

‡ Department of Biochemistry, Cellular and Molecular Biology.

§ Graduate School of Genome Science and Technology.

[1] Abbreviations: DHFR, dihydrofolate reductase; wt, wild type; TMP, trimethoprim; DHF, dihydrofolate; $NADP^+$ and NADPH, oxidized and reduced nicotinamide adenine dinucleotide phosphate, respectively; NMN, nicotinamide mononucleotide; MTA buffer, 100 mM Tris, 50 mM MES, 50 mM acetic acid polybuffer; ITC, isothermal titration calorimetry. Mutant enzymes containing amino acid substitutions are described by the wild-type residue and numbered position in the sequence, followed by the amino acid substitution. For example, V66A R67 DHFR describes the Val66 → Ala mutant.

10.1021/bi049646k CCC: $27.50 
Published on Web 05/20/2004

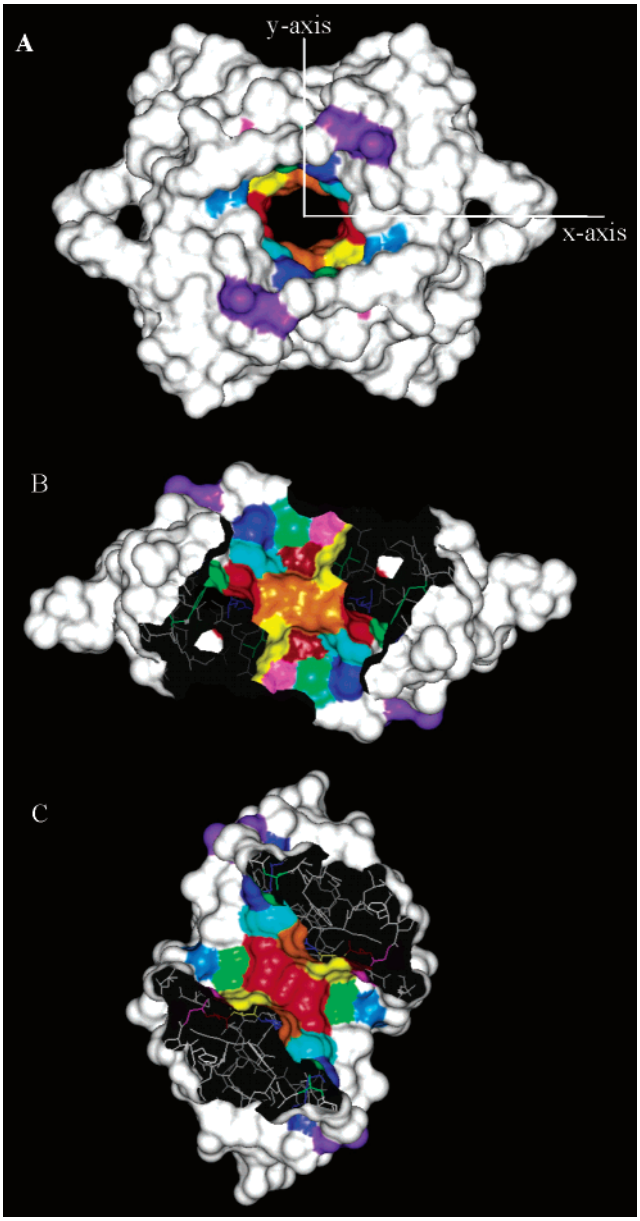


FIGURE 1: Connolly surfaces of R67 DHFR. Panel A shows the entire tetramer looking along the *z*-axis into the active site pore. Active site residues are colored as follows: dark blue for K32, purple for K33, light green for A36, green for Y46, sky blue for T51, magenta for G64, brick red for S65, yellow for V66, orange for Q67, red for I68, and cyan for Y69. Panel B depicts the dimer−dimer interface (only one is shown), which occurs on the "top" and "bottom" of the active site pore. The orientation is related to that in panel A by a 90° rotation about the *x*-axis. Two symmetry-related Q67 residues interact and form the continuous orange patch. Panel C describes the monomer−monomer interface (only one is shown), which occurs on the "sides" of the pore. The orientation is generated from panel A by a 90° rotation about the *y*-axis. Two symmetry-related I68 residues interact and form the continuous red patch.

of folate displays positive cooperativity ($K_d$ values of 195 and 48 $\mu$M). Positive cooperativity between bound NADPH and folate also exists, establishing a preferred catalytic path where the free enzyme binds the cofactor first, followed by substrate which forms the productive ternary complex (*8*). These results indicate each half of the pore can bind either NADPH and $NADP^+$ or folate and DHF.

To obtain a model of the productive ternary complex, NMR and docking approaches have been used (*9*−*11*). Few interligand nuclear Overhauser effects (ILOEs) are observed between $NADP^+$ and folate, consistent with the ligands entering the pore from opposite sides and meeting at the middle (*11*). Backbone and side chain NMR assignments indicate the most strongly shifted resonances upon $NADP^+$ binding describe K32, K33, G35, E39, S59, E60, A61, G64, S65, V71, A72, A73, and L74 residues[2] (*9*). Using constraints derived from NMR as well as the stereochemistry of the reaction, docking studies predict a model of bound NMNH (reduced nicotinamide mononucleotide) that interacts with the pteridine ring of folate (Fol I from 1VIF) at the pore's center (*10*). Numerous residues serve dual roles in binding. For example, Gln67 from both the B and D subunits has several contacts with the pteridine ring, while the same residue from the A and C subunits has several contacts with the nicotinamide ring. The residues involved in dual roles are generally amphipathic, allowing them to make both hydrophobic and hydrophilic contacts with the ligands. The result is a "hot spot" binding surface that allows the same residues to co-optimize the binding of two ligands, and orient them for catalysis. A docked model for the NADPH·folate ternary complex is shown in Figure 2.

To evaluate this ternary complex model, site-directed mutagenesis has been employed. Residues that make up the pore have been identified using CAST, an algorithm that identifies cavities (*12*; see http://cast.engr.uic.edu/cgi-bin/cast1/index.pl). These residues include K32, K33, S34, G35, A36, Y46, T48, L50, T51, G64, S65, V66, Q67, I68, Y69, P70, and A73. Numerous residues near the center of the pore were previously mutagenized (S65, Q67, I68, and Y69), and substantial effects on binding and catalysis were noted [except for S65 (*1*, *3*)]. The roles of K32 and K33, located near the edge of the pore, were evaluated by mutagenesis and salt effects (*2*). K33 plays a minor role in binding, while K32 appears to be the key player in facilitating binding of the negatively charged ligands, DHF and NADPH. This study continues a mutagenesis approach to evaluating the docked ternary complex model in which residues farther out on the pore surface have been mutagenized. Those residues that are predicted to interact with bound ligand have been targeted, including A36, Y46, T51, G64, and V66.

The predicted H-bond and van der Waals interactions with docked NADPH include a close pairing between the OG1 atom of T51 and the N7 atom from the adenine ring, a close contact between the backbone oxygen of G64 with the N6 and C6 atoms of the adenine moiety, and a juxtaposition of the backbone oxygen of V66 near the C5 atom of the nicotinamide moiety (*10*). Also, the CB atom of A36 has been suggested to be in the proximity of the C2 and N3 atoms of adenine. For DHF docking, the backbone oxygen of V66 has been predicted to interact with the hydrogen on N5 of the pteridine ring. Although these interactions describe contacts for the top-scoring conformers, Y46 is predicted to hydrogen bond with the substrate when additional scoring conformers are considered.

[2] The amino acids in the first monomer are labeled 1−78, those in the second monomer 101−178, those in the third monomer 201−278, and those in the fourth monomer 301−378. For brevity, when a single residue is mentioned, all four symmetry-related residues are implied.

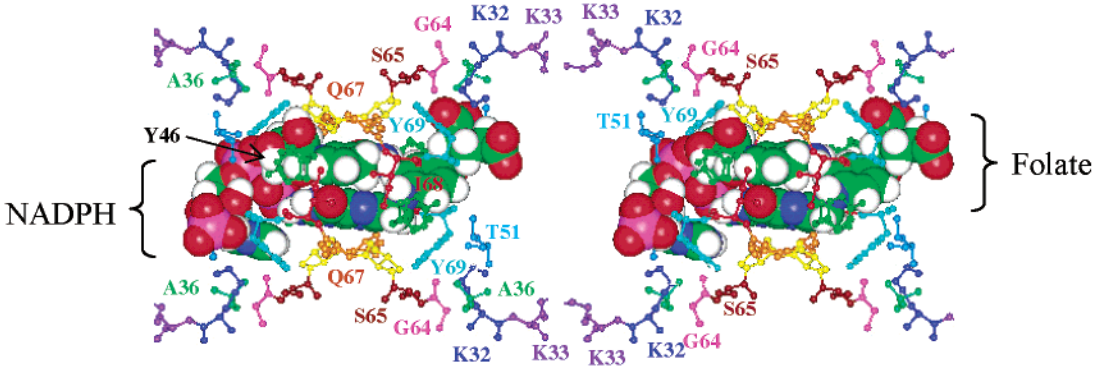


FIGURE 2: Stereoview of the docked model for the R67 DHFR·NADPH·folate ternary complex generated by DOCK (*10*). This view of the active site corresponds to that seen in Figure 1C, where the active site pore has been rotated 90° about its *y*-axis. The pteridine ring of bound folate (FolI) from the crystal structure of R67 DHFR (1VIF) was used to dock the nicotinamide−ribose−$P_i$ (NMNH) moiety of NADPH as well as NADPH itself. Interligand NOEs derived from NMR experiments as well as the A-side stereochemistry of the reaction (*11*, *26*, *57*, *58*) were used to evaluate the dockings. Since the *p*-aminobenzoylglutamic acid (pABA-Glu) tail of FolI is disordered in the crystal structure, FolI was then removed from the top-scoring FolI·NMNH ternary complex and the full-length folate molecule was docked. Of the top 25 scoring orientations, 21 placed the pteridine ring of folate in the same general position as FolI, while the position of the pABA-Glu tail of folate varied. The top-scoring folate conformer is shown at the top right using a CPK surface. The only docked NADPH molecule that met the NMR constraints (nicotinamide ring is *syn* with respect to its ribose ring and the adenine ring *anti* with respect to its ribose) is depicted at the bottom left, also using a CPK surface. Stacking between the pteridine ring of folate and the nicotinamide ring of NADPH can be seen in the central part of the figure. For the ligands, the color code is as follows: green for carbon, blue for nitrogen, red for oxygen, magenta for phosphorus, and white for hydrogen. The active site residues in R67 DHFR are shown using ball-and-stick representations, and color-coded labels are provided. The color scheme is the same as in Figure 1. Val66 residues are yellow and are unlabeled. Since Ile68 (red) and Tyr46 (green) residues occur on the side of the active site, two pairs of these side chains can be seen near the side of the ligands, while two symmetry-related pairs are hidden behind the ligands.

This mutagenesis series, in combination with previous studies (*1*−*3*), identifies the set of contiguous residues that are important in binding and catalysis. Finally, formation of the ternary complex was studied using isothermal titration calorimetry, and a correlation between $\Delta H$ and $k_{cat}/K_m$ has been noted.

## MATERIALS AND METHODS

*Construction and Expression of Mutant R67 DHFRs.* A synthetic R67 DHFR gene, carried in pUC8, has been previously described (*6*). Site-directed mutagenesis using the appropriate primers was employed to construct A36S, Y46F, Y46H, T51V, T51S, G64A, V66A, and V66T mutations in the R67 DHFR gene by the PCR-based protocol outlined in the Quikchange kit from Stratagene. The PCR-based reactions, used in site-directed mutagenesis, required two complementary oligonucleotide primers containing the desired mutation. The coding strand sequences for each nucleotide primer are as follows: 5′-CGTAAGAAATCCGGC(**TCC)**GCCTGGCAAGGTC-3′ for A36S, 5′-CAGATTGTCGGGTGG(**TTC)**TGCACAAATTTGACCC-3′ for Y46F, 5′-CAGATTGTCGGGTGG(**CAC)**TGCACAAATTTGACCC-3′ for Y46H, 5′-GCACAAATTTG(**GTC)**CCCGAGGGCTACG-3′ for T51V, 5′-CTGCACAAATTTG(**AGC**)CCAGAGGGCTAC-3′ for T51S, 5′-CAGGATAGATCTGTACTGA(**CGC)**CGGGTGAGCCTCAGAC-3′ for G64A, 5′-GCTCACCCGGGCTCA(**ACA**)CAGATCTATCCTGTTGC-3′ for V66T, and 5′-GCTCACCCGGGCTCA(**GCA**)CAGATCTATCCTGTTGC-3′ for V66A.

When feasible, concurrent changes of restriction sites allowed ready identification of mutants. To confirm the mutation and to determine that no extraneous mutations occurred in the R67 DHFR gene, the DNA was sequenced using an ABI PRISM Dye Terminator Cycle Sequencing Ready Reaction kit from Perkin-Elmer (University of Tennessee Sequencing Facility).

*Escherichia coli* cells (strain SK383) containing the mutant genes were grown to late stationary phase in the presence of 200 $\mu$g/mL ampicillin. TMP (20 $\mu$g/mL) was added if the gene conferred TMP resistance upon host *E. coli.* Cells were lysed using an alkaline lysis method, and the protein was purified to homogeneity using standard chromatography steps (*6*).

*Steady-State Kinetics.* Steady-state kinetic data were obtained using a Perkin-Elmer $\lambda$3a spectrophotometer interfaced with an IBM PS2 computer as previously described (*13*). Briefly, assays were performed at 30 °C in a polybuffer containing 50 mM MES, 100 mM Tris, and 50 mM acetic acid at pH 7 (MTA buffer) (*14*). This polybuffer maintains a constant ionic strength from pH 4.5 to 9.5. Assays were performed by the addition of substrate (DHF) and cofactor (NADPH), followed by the addition of the enzyme to initiate the reaction. To obtain $k_{cat}$ and $K_m$ values for each mutant, the concentration of NADPH was held constant at a subsaturating level, while the concentration of DHF was varied. This process was repeated using four additional subsaturating concentrations of NADPH. The data were fit globally to the nonlinear bisubstrate Michaelis−Menten equation utilizing SAS [statistical analysis software (*15*)]. The NLINEK macro for use in SAS is available at http://www.agriculture.utk.edu/ansci/faculty/saxton_software.html. When NADH was used as an alternate cofactor, substrate inhibition was observed. The resulting data were fit to a revised bisubstrate equation containing terms describing formation of a two-DHF complex (*8*, *15*).

Protein and ligand concentrations were determined spectrophotometrically. For all mutants, extinction coefficients were determined using the biuret assay (*16*). Ligand concentrations were determined using the following extinction coefficients: 28 000 $M^{-1}$ $cm^{-1}$ at 282 nm for DHF (*17*) and 6220 $M^{-1}$ $cm^{-1}$ at 340 nm for NADPH (*18*). The molar extinction coefficient used to assess DHFR reduction of DHF

and NADPH was 12 300 $M^{-1}$ $cm^{-1}$ (*19*).

*Isothermal Titration Calorimetry.* Binding affinities, stoichiometries, and the enthalpy associated with binding were monitored using isothermal titration calorimetry (ITC) as previously described (*8*). Binding of ligands to R67 DHFR variants was assessed using a Microcal VP isothermal titration calorimeter. The data were automatically collected with an IBM personal computer running DSCITC data acquisition software and were analyzed using Origin provided by the manufacturer. The design and operation of this instrument have been described by Wiseman *et al*. (*20*). Unless otherwise indicated, samples typically consisted of 90−240 $\mu$M tetramer in MTA buffer (pH 8). For binary experiments in which NADPH was monitored as a titrant, measurements were performed at 28 °C. Addition of ligand to buffer allowed baseline corrections. Binary data sets were fit to an interacting sites model where the stoichiometry of ligand binding was set equal to 2. For studying binding of folate to the R67 DHFR·NADPH complex (or the R67 DHFR·NADH complex), experiments were performed at 13 °C to minimize catalysis. In these experiments, the protein and NADPH were added to the sample cell at a 1:1 ratio, while the protein and NADH were added at a 1:3 ratio. Folate was then titrated into the sample until saturation was achieved. The ternary data were fit to a single-site model.

*pH Titration of Tryptophan Fluorescence.* To determine whether the active site mutations in this study affect the overall oligomeric structure, steady-state tryptophan fluorescence was used to monitor the pH-dependent equilibrium between the tetramer and two protonated dimers in either wild-type or mutant R67 DHFRs given by

$$T + 2nH^+ \overset{K_{overall}}{\rightleftharpoons} 2DH_n$$

where T is the tetramer, $DH_n$ is the protonated dimer, $2n$ is the number of protons, and $K_{overall}$ equals $([T][H]^{2n})/[DH_n]^2$ (*21*). The emission spectra for the DHFRs (excitation at 295 nm) were measured from 300 to 450 nm at each pH during the titrations. The intensity-averaged emission wavelength, $\langle\lambda\rangle$, for each emission spectrum was calculated using $\langle\lambda\rangle = \sum(I_i\lambda_i)/\sum(I_i)$, where $I$ is the intensity and $\lambda$ is the wavelength (*22*). $\langle\lambda\rangle$ is an integral measurement that is less sensitive to noise. Data were fit to the following equation describing the linkage between the tetramer and protonated dimer equilibrium (*21*):

$$Flu_{obs} = (Flu_{di} - Flu_{tet})[[H]^{2n}/(4K_{overall}P_{tot})][-1 + (1 + 8K_{overall}P_{tot}/[H]^{2n})^{1/2}] + Flu_{tet} \quad (1)$$

where $K_{overall} = ([T][H]^{2n})/DH_n^2$ in units of M, $M^2$, or $M^3$ for $n = 1$, 1.5, or 2, respectively, $Flu_{obs}$ is the observed fluorescence, $Flu_{di}$ and $Flu_{tet}$ are the calculated limits for dimer and tetramer fluorescence at low and high pH values, respectively, and $P_{tot}$ is the total protein concentration in terms of the dimer (*21*). SAS was employed to fit the data using nonlinear regression.

## RESULTS

The A36S, Y46F, Y46H, T51V, T51S, G64A, V66A, and V66T R67 DHFR mutant genes were constructed and sequenced. To evaluate which mutations were most functional, *E. coli* cells were transformed with plasmid DNA containing the mutant genes and screened for the ability to confer resistance to trimethoprim. Only Y46F, Y46H, T51S, V66A, and V66T mutant genes provided resistance to the antibiotic at 20 $\mu$g/mL. The A36S and T51V mutant genes did not confer resistance to TMP upon host *E. coli.* As other mutants with this phenotype have typically resulted in an inactive, dimeric protein, we did not pursue these mutants further. The protein yields for the Y46H and G64A mutants were negligible and thus not characterized.

Table 1: Best Fit Values for the pH-Dependent Tetramer ⇄ Two-Protonated Dimer Dissociation As Monitored by Fluorescence

| DHFR species | $K_{overall}$ ($=K_a^{2n}/K_d$) for $2n = 3$ ($M^2$) |
|---|---|
| wt R67 DHFR | $1.2 \times 10^{-13} \pm 4.0 \times 10^{-14}$ |
| Y46F R67 DHFR | $9.3 \times 10^{-14} \pm 2.1 \times 10^{-14}$ |
| T51S R67 DHFR | $1.3 \times 10^{-13} \pm 1.8 \times 10^{-14}$ |
| V66A R67 DHFR | $1.1 \times 10^{-13} \pm 3.0 \times 10^{-14}$ |

Table 2: Comparison of Steady-State Kinetic Values for R67 DHFR Variants at pH 7.0

| DHFR species | $k_{cat}$ ($s^{-1}$) | $K_{m(DHF)}$ ($\mu$M) | $K_{m(cofactor)}$ ($\mu$M) |
|---|---|---|---|
| wt R67 DHFR[a] | 1.3 ± 0.1 | 5.8 ± 0.02 | 3.0 ± 0.1 |
| Y46F R67 DHFR | 1.2 ± 0.1 | 7.0 ± 0.4 | 4.0 ± 0.2 |
| T51S R67 DHFR | 0.6 ± 0.1 | 6.4 ± 0.4 | 3.8 ± 0.2 |
| V66A R67 DHFR | 1.4 ± 0.1 | 7.6 ± 0.01 | 6.3 ± 0.03 |
| V66T R67 DHFR | 0.44 ± 0.004 | 4.0 ± 0.1 | 7.3 ± 0.20 |
| Y69L R67 DHFR | 0.16 ± 0.01 | 180 ± 11 | 68 ± 3 |
| wt R67 DHFR with NADH[b] | 0.093 ± 0.01 | 25 ± 3 | 11 ± 6 |

[a] Values from ref *6*. [b] Steady-state kinetics using NADH as a cofactor.

*pH Titration of Tryptophan Fluorescence.* To probe whether the mutations alter the pH dependence of the oligomeric state of R67 DHFR, steady-state tryptophan fluorescence was monitored as a function of pH (*21*). Symmetry-related H62, H162, H262, and H362 residues located at the dimer interfaces stabilize tetrameric R67 DHFR. Titration of these residues results in tetramer destabilization and formation of protonated dimers. Since W38 also occurs at the dimer−dimer interfaces, tryptophan fluorescence can be used to monitor whether the W38 environment is solvent-exposed (dimer) or buried in a more hydrophobic environment (tetramer) (*23*). The $K_{overall}$ values ($=K_a^{2n}/K_d$) obtained from the pH titration data for wt, Y46F, T51S, and V66A R67 DHFRs are listed in Table 1. These values are all similar to those for wt R67 DHFR with the best fit occurring when $2n = 3$, where $2n$ represents the number of protons added to the dimer−dimer interfaces resulting in dissociation of the tetramer. The data indicate that the Y46F, T51S, and V66A mutations minimally perturb the equilibrium between the tetramer and two dimers.

*Steady-State Kinetic Analysis.* Steady-state kinetic data are presented in Table 2 for wt and mutant R67 DHFRs. The kinetic values for the Y46F, T51S, and V66 mutants are comparable (within a factor of 2) to those of wt R67 DHFR. For Y46 substitutions, the Y46F mutant was conservative while the Y46H mutation was not. The Y46H mutant expression levels were negligible.

*Isothermal Titration Calorimetry.* Isothermal titration calorimetry (ITC) measures the amount of heat released or

Table 3: Comparison of Macroscopic $K_d$ Values Describing Binding of NADPH to R67 DHFR Variants Monitored by ITC[a]

| DHFR species | $K_d$ ($\mu$M) | $\Delta H$ (kcal/mol) | no. of experiments |
|---|---|---|---|
| wt R67 DHFR[b] | $2.5 \pm 0.2$ | $-8.6 \pm 0.1$ | 2 |
| | $95 \pm 4$ | $-5.8 \pm 2.5$ | |
| Y46F R67 DHFR | $6.0 \pm 0.1$ | $-7.8 \pm 0.1$ | 2 |
| | $120 \pm 0.3$ | $-5.3 \pm 0.1$ | |
| T51S R67 DHFR | $2.6 \pm 0.6$ | $-8.4 \pm 0.3$ | 2 |
| | $87 \pm 20$ | $-3.7 \pm 0.4$ | |
| V66A R67 DHFR | $3.2 \pm 0.1$ | $-9.5 \pm 0.1$ | 2 |
| | $120 \pm 3$ | $-6.6 \pm 0.2$ | |
| wt R67 DHFR titrated with NADH | $21 \pm 0.9$ | $-10.0 \pm 0.2$ | 2 |
| | $180 \pm 12$ | $-1.4 \pm 0.2$ | |

[a] Values reported for all mutants are fit to an interacting sites model that sets the ligand stoichiometry at 2.0. [b] From ref *8*.

absorbed upon binding of a ligand to a protein or other macromolecule. To determine the effect of the mutations on ligand binding and cooperativity, isothermal titration calorimetry was employed to monitor binding of NADPH to the Y46F, T51S, and V66A DHFRs. Wild-type R67 DHFR binds two NADPH molecules, with negative cooperativity (*8*). Best fit values associated with titrating the mutant proteins with NADPH are given in Table 3. In agreement with the steady-state kinetic data described above, the mutations do not alter NADPH binding greatly.

From previous studies, it has been observed that titrating folate (a poor substrate of R67 DHFR) into a sample cell containing a 1:1 ratio of protein and NADPH results in an exothermic binding isotherm (*8*). We have, therefore, used this method to monitor binding of folate to various mutant protein·NADPH complexes. Figure 3 shows a representative ITC titration for formation of a ternary complex between a 1:1 mixture of I68M R67 DHFR and NADPH titrated with folate. ITC data for a series of mutants possessing different $k_{cat}/K_m$ values are given in Table 4 and plotted in Figure 4. Other mutants, from a previous study (*1*) in which steady-state kinetic data were collected, have been studied by ITC, and their enthalpies of binding are presented as well. From these data, differences in $\Delta H$ are seen for mutants with different $k_{cat}/K_m$ values. For example, Q67C R67 DHFR has a $k_{cat}$ of 0.10 $s^{-1}$ and a binding enthalpy corresponding to $-0.99$ kcal/mol. Y46F R67 DHFR has a $k_{cat}$ value of 1.2 $s^{-1}$ and a binding enthalpy of $-9.0$ kcal/mol. To probe whether the linear correlation continued with another mutant possessing very low activity, Y69L R67 DHFR was also included. Mutant details will be given by Stinnett *et al.* (manuscript submitted to the *Journal of Biological Chemistry*), although $k_{cat}$, $K_m$, $K_d$, and $\Delta H$ values are given in Tables 2 and 4.

Since folate is a poor substrate for R67 DHFR, an issue is whether some minimal reduction could occur during these titrations. However, previous studies found the $k_{cat}$ for folate reduction at pH 8 (20 °C) to be 0.0036 $min^{-1}$ (*8*). While this rate is quite low, it still might contribute to some level of catalysis during the titrations, which take 2−3 h to complete. Therefore, these titrations were performed at 13 °C to further decrease the rate. Since the wt enzyme is the most active species, it is pertinent that additional studies using wt R67 DHFR have found that two control points within 5 min of each other at folate concentrations of 1 and 200 $\mu$M display the same relative position on the titration curve as seen in the longer 2−3 h data set (*8*). This observation indicates that any contribution of catalysis to the binding curve in wt R67 DHFR is minimal. Since the mutants display decreased activity, weaker effects would be expected in their titrations.

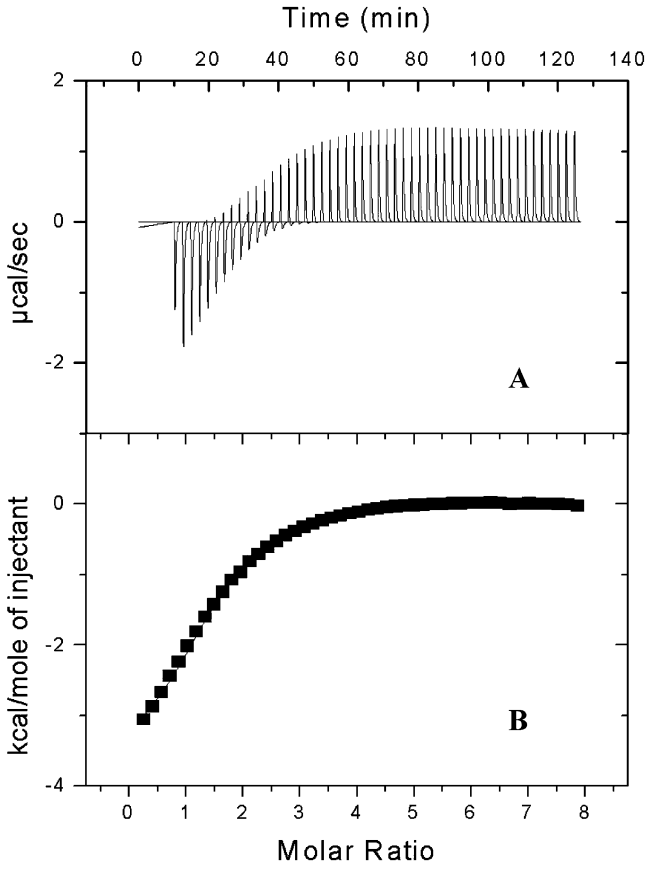


FIGURE 3: Formation of a ternary complex between a 1:1 mixture of I68M R67 DHFR and NADPH titrated with folate. The initial protein concentration was 124 $\mu$M. Although folate is a poor substrate for R67 DHFR, a limited reduction of folate could potentially occur. Therefore, this experiment was carried out at 13 °C and pH 8 to minimize catalysis. Additional control studies (see the text) suggest a minimal contribution of folate reduction to catalysis. Panel A represents the series of peaks generated with each addition of ligand. Panel B shows the heat liberated per mole of titrant added vs the folate:protein tetramer molar ratio.

Table 4: Ternary Complex Formation Monitored by ITC[a]

| DHFR species | $K_d$ ($\mu$M) | $\Delta H$ (kcal/mol) | stoichiometry | no. of experiments |
|---|---|---|---|---|
| wt R67 DHFR[b] | $11 \pm 0.1$ | $-8.6 \pm 0.1$ | $0.87 \pm 0.02$ | 4 |
| Y46F R67 DHFR | $14 \pm 0.3$ | $-9.0 \pm 0.3$ | $0.83 \pm 0.02$ | 2 |
| T51S R67 DHFR | $10 \pm 0.9$ | $-6.6 \pm 0.2$ | $0.69 \pm 0.01$ | 3 |
| V66A R67 DHFR | $12 \pm 0.3$ | $-8.5 \pm 0.1$ | $0.92 \pm 0.01$ | 2 |
| Q67C R67 DHFR[c] | $57 \pm 8$ | $-0.99 \pm 0.06$[d] | $0.86 \pm 0.04$ | 2 |
| I68L R67 DHFR[c] | $48 \pm 5$ | $-5.4 \pm 0.5$ | $0.85 \pm 0.06$ | 2 |
| I68M R67 DHFR[c] | $43 \pm 4$ | $-4.5 \pm 0.1$ | $1.3 \pm 0.03$ | 2 |
| Y69L R67 DHFR[e] | $86 \pm 4$ | $-3.9 \pm 0.2$ | $0.96 \pm 0.03$ | 2 |
| wt R67 DHFR with NADH | $40 \pm 1.3$ | $-3.9 \pm 0.08$ | $0.94 \pm 0.02$ | 2 |

[a] Folate was titrated into a 1:1 mixture of enzyme and NADPH at 13 °C to minimize catalysis. The last row describes titration of folate into a 1:3 mixture of enzyme and NADH. [b] From ref *8*. [c] Mutants constructed in ref *1*. [d] Since this value is so small, it likely has a greater error in it than that indicated, as the background "noise" associated with dilution of folate begins to contribute more to the overall signal. [e] Mutant details to be published by Stinnett *et al.* (manuscript submitted to the *Journal of Biological Chemistry*).

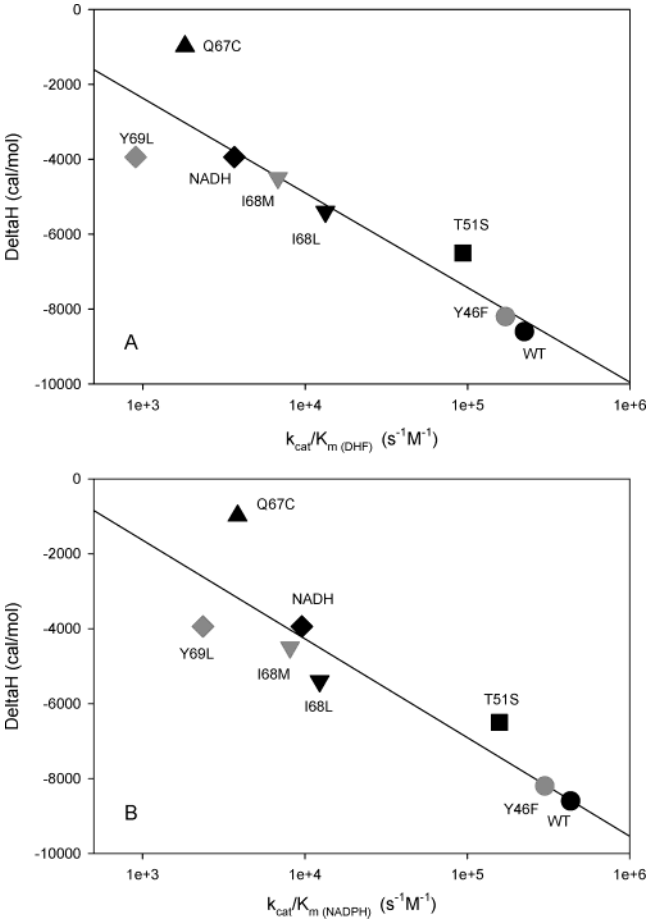


FIGURE 4: Potential linear correlation between the heat of enthalpy for binding of folate to the R67 DHFR·NADPH complex (pH 8) and log $k_{cat}/K_m$ (pH 7). Panel A depicts the correlation for $k_{cat}/K_{m(DHF)}$, while panel B depicts the $k_{cat}/K_{m(NADPH)}$ data. Values for $\Delta H$ are listed in Table 4. Values for $k_{cat}$ and $K_m$ come from Table 2 or from Strader *et al.* (*1*). While the data points are labeled, the code is as follows: wild-type R67 DHFR (●), Y46F (gray circles), T51S (■), I68L (▼), I68M (gray triangles), NADH (◆), Y69L (gray diamonds), and Q67C (▲).

To examine whether the linear correlation extends to alternate ligands, NADH was used as a cofactor. The isotherm for NADH binding under binary complex conditions can be fit with either a one- or two-site model. The fit for the two-site model is given in Table 3. The first $K_d$ for the two-site model is 21 $\mu$M (~9-fold higher than the $K_d$ for NADPH). The second $K_d$ for this model is typically 100−200 $\mu$M, consistent with negative cooperativity. However, this second $K_d$ varies depending on the data set and is just at the limit of the suggested *c* value (=[total protein]/$K_d$) range (1−1000), suggesting binding is weak and that it is difficult to determine this $K_d$ with a small error (*20*). The $K_d$ from fitting this same data set to the single-site model is 38 $\mu$M (an ~2-fold increase from that of the two-site model).

Ternary complex formation using NADH is not as straightforward. For example, a titration typically starts with a 1:1 mixture of cofactor and protein, which allows formation of the R67 DHFR·cofactor complex. Addition of folate then leads to the ternary complex. However, for a 1:1 mixture of NADH and R67 DHFR, titration of folate results in an isotherm with a hook, indicative of positive cooperativity and binding of more than one folate molecule. This result suggests initial binding of folate to the R67 DHFR·NADH complex, followed by displacement of NADH and generation of a two-folate complex. This observation also corroborates steady-state kinetic data (ref *2* and below) where DHF inhibition readily occurs at low NADH concentrations (i.e., formation of a two-DHF complex). The ternary complex values in Table 4 were therefore generated using a 3:1 ratio of NADH to enzyme. A 3.6-fold increase in the $K_d$ is observed when this $K_d$ is compared to that for formation of the NADPH·folate complex, and, most interestingly, a substantial decrease in the associated enthalpy.

As noted previously by Hicks *et al.* (*2*), steady-state kinetics using NADH as a cofactor show DHF inhibition at low salt concentrations. Since fitting data sets displaying inhibition (by SAS) requires some knowledge of the various $K_d$ values that are involved, we used the ITC values given above. In the fitting process, the input $K_d$ values were allowed to vary 2−3-fold. The best fit for $K_{d(NADH)}$ was 43 ± 6 $\mu$M, agreeing with the fit of binary NADH data to a single-site model. The steady-state kinetics data are shown in Figure 5, and the fit values are given in Table 2. When added to Figure 4, the resulting data point contributes to the linear trend, suggesting that looseness of binding (derived from either alternate ligands or protein mutations) controls catalytic efficiency.

## DISCUSSION

*Effects of Mutations.* Since R67 DHFR is one of the smallest proteins to form an active enzyme [see oxalocrotonate tautomerase as another example, with 62 amino acids per monomer (*24*)], this likely leads to a multitasking approach in the structure−function relationship. In this scenario, each residue can participate in a number of roles, including contributions to folding, stability, and oligomerization state as well as binding and catalysis. This issue suggests that single mutations in the R67 DHFR gene which result in four mutations per homotetramer can readily lead to large cumulative effects. This issue clearly comes into play with the A36, T51, and G64 mutants studied in this report.

From our studies, A36S and T51V mutant genes do not confer resistance to TMP while the Y46H and G64A mutant proteins have low expression levels. A36 is at the dimer−dimer interface. Both A36 and G64 are parts of turns, while T51 is between a turn and a proline. Mutations of these residues could very well compromise the structural ability of the turn to form, leading to either a folding, stability, or oligomerization problem. Only the conservative T51S and Y46F mutants as well as mutants at V66 resulted in active proteins that could be characterized.

The most conservative mutation at T51 results in a fully active protein. Since the side chain hydroxyl was proposed as the functional group from docking studies, this report finds that any difference in rotamer populations (*25*) associated with threonine versus serine at this position does not affect binding and catalysis.

Both Y46 and V66 occur on the "sides" of the active site pore, with V66 near the center and Y46 further out on the binding surface (Figures 1 and 2). V66 presents its backbone amide and oxygen as well as side chain atoms for interaction, while Y46 presents only its side chain CE2 and OH atoms. None of the V66 mutants altered kinetic or ITC values

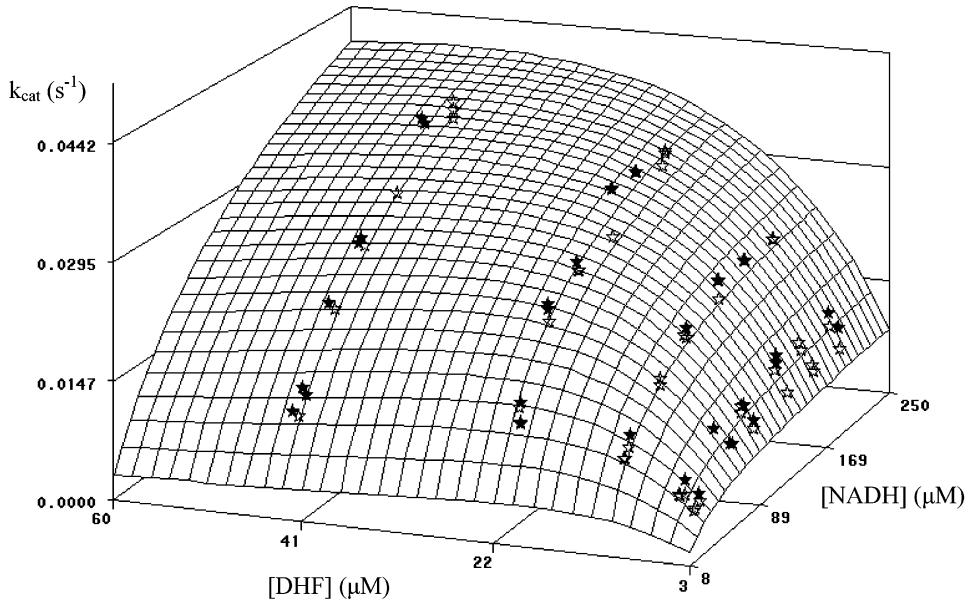


FIGURE 5: Three-dimensional plot of steady-state kinetic data using NADH as a cofactor. Data were fit to an equation describing bisubstrate kinetics along with formation of a nonproductive two-DHF complex using SAS (*15*). Data points above and below the calculated three-dimensional plot are depicted with filled and empty stars, respectively.

significantly, indicating that V66 residues do not directly interact with either NADPH or DHF or, if the interaction utilizes an intermediate water, the water position is not altered. A third possibility is that if the interactions use backbone interactions, the substitution does not affect the backbone position. For the Y46F mutant, no substantial changes in activity were observed, suggesting the hydroxyl group does not play a role in binding (with the above caveats). For the less conservative Y46H mutant, protein yields were negligible, suggesting the substitution alters packing in the hydrophobic core and thus protein stability.

*Residues that Compose the Ligand Binding Surface of R67 DHFR.* While the conservative mutants constructed in this study minimally affect the catalytic activity of R67 DHFR, we are now able, in conjunction with our previous mutagenesis studies (*1*−*3*), to delineate the residues that comprise the binding surface. K32, Q67, I68, and Y69 appear to be the most important residues involved in ligand binding and catalysis. First, Delphi predictions indicate positively charged K32 residues create a positive electrostatic potential in the active site pore that serves to attract the negatively charged cofactor and substrate (*10*). The role of K32 is further supported by salt effect studies indicating that this residue is important in both binding and catalysis (*2*). Second, steady-state kinetic and ITC data clearly indicate that mutations at residues Q67, I68, and Y69 result in profound changes in both ligand binding affinity and catalysis (*1*, *3*, *15*). Finally, mutations at positions K33, Y46, S65, and V66 result in mutants with <5-fold effects on binding and catalysis (*1*, *2*).

Only 42% of the surface area in the active site pore is contributed by residues K32, Q67, I68, and Y69 (total surface area calculated by CAST). These residues are highlighted in blue in Figure 6. The surface for symmetry-related K32, Q67, I68, and Y69 residues comprises two continuous strips that run from one edge of the pore to the other (only one is shown). While residues Q67, I68, and Y69 would be expected to be near each other, the contiguous placement of

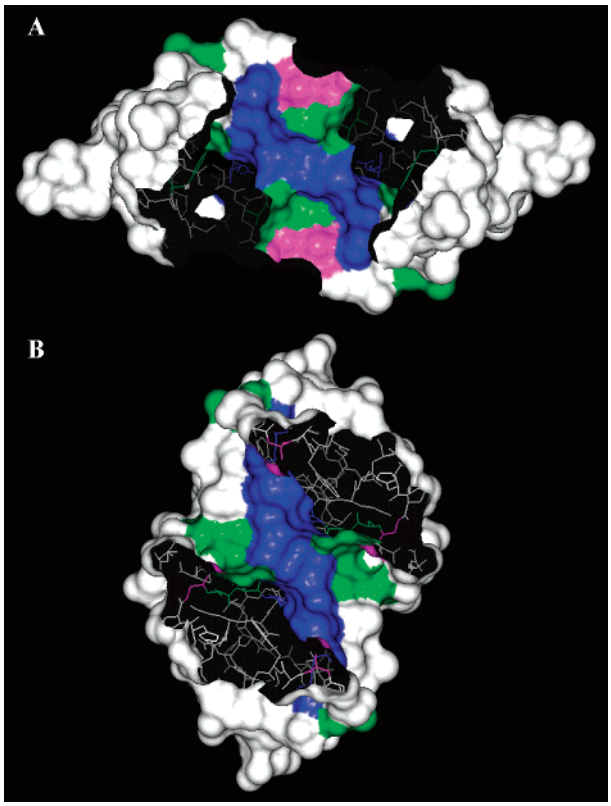


FIGURE 6: (A) Depiction of a single dimer−dimer interface in R67 DHFR. (B) Depiction of a single monomer−monomer interface. These are the same orientations as in panels B and C of Figure 1, respectively. Residues for which conservative mutations displayed a >5-fold effect are colored blue (K32, Q67, I68, and Y69). Residues for which conservative mutations displayed no to minimal effects are colored green (K33, Y46, T51, S65, and V66). Residues for which mutations apparently perturbed the quaternary and/or tertiary structure are colored magenta (A36 and G64).

K32 in this strip supports its importance in binding and catalysis. Conversely, the pore surface area contributed by residues K33, Y46, T51, S65, and V66 to the pore totals 30%. These residues also form symmetry-related contiguous

clusters (two are shown in green), suggesting these areas are not directly involved in ligand binding. Residues that apparently alter the ability of the protein to fold or oligomerize are shown in magenta.

One observation concerning this "map" of the active site pore is that the hourglass center appears to be critical (from Q67 and I68 contributions). This strategy may allow the ligands to approach each other from opposite ends of the pore and find the correct orientation for catalysis with minimal water access. Mutations in this area could result in altered stacking of the ligands as well as poor alignment for hydride transfer.

This map agrees qualitatively with that obtained by Pitcher *et al*. (*9*), in which the NMR chemical shift data were plotted over the protein backbone. In general, those data show the largest changes in chemical shifts upon $NADP^+$ binding occur in the pore with smaller shifts occurring in a secondary sphere around the active site. Their study suggested a subtle structural adjustment to $NADP^+$ binding which might slightly perturb the $\beta$-sheet structure.

*What Is the Catalytic Strategy of R67 DHFR?* The 222 symmetry of the structure, the single active site pore, the formation of nonproductive complexes, and the lack of a suitable general acid catalyst (*26*) clearly indicate that R67 DHFR provides a catalytic strategy very different from those of most enzymes and chromosomal DHFR in particular. Because of these features, R67 DHFR may be an ideal model of a primitive enzyme that has not yet been optimized by evolution.

ITC, kinetic, and computational data indicate that R67 DHFR has a "one site fits both" binding strategy in which three possible combinations of bound ligands have been observed. One of these leads to catalysis, while the other two nonproductive complexes (two NADPH and two DHF molecules) block the active site pore. Interligand interactions, therefore, appear to be important in this enzyme and provide a productive strategy for formation of the transition state.

ITC experiments allow evaluation of the hypothesis described above by monitoring the enthalpy associated with binding of folate to the R67 DHFR·NADPH complex using various mutants. A trend that is noted is a linear correlation between $\Delta H$ and $k_{cat}/K_m$ in a semilog plot (Figure 4). The trend is extended when the alternate cofactor, NADH, is included. These data are consistent with higher catalytic efficiencies being correlated with an increasing exothermicity of ternary complex formation. The range includes ~200−250-fold effects on $k_{cat}/K_m$ and 8 kcal/mol differences in $\Delta H$. These results point to an enthalpic basis being associated with the positive cooperativity between the cofactor and folate in binding. Increased exothermicity has been proposed to be associated with noncovalent interactions that result in a tighter interface or closer contact distances (*27*−*29*). The $k_{cat}/K_m$ values for various mutants (and NADH) may therefore be correlated with interligand contact distance, assuming no large change in orientation. For R67 DHFR, the closer the contact distance, the better the catalytic efficiency.

Preorganization of an enzyme's active site is proposed as being crucial in numerous theories for formation of the transition state (*30*−*33*). Perhaps R67 DHFR employs this strategy, although with an emphasis on optimizing interligand interactions, which ultimately lead to the transition state. The data in Figure 4 support this idea, as a correlation between ground-state binding and catalytic efficiency is observed. If a more negative $\Delta H$ value correlates with a shorter contact distance (*27*−*29*), then the wt enzyme has evolved to provide a reasonable approach to catalyzing the DHFR reaction using this scaffold. In addition, use of the alternate cofactor NADH lacking the 2′-phosphate moiety also leads to poorer catalysis, presumably because it is not as preorganized a binding partner [previous studies suggest an interaction between the 2′-phosphate of NADPH and K32 in R67 DHFR (*2*)].

Figure 4 also supports the hypothesis that R67 DHFR utilizes an *endo* transition state (where the nicotinamide ring overlaps with the more bulky side of the pteridine ring) rather than the *exo* conformer (with minimal overlap of the two ligands). Previously, this view arose from interligand NOE NMR data (*11*) and docking studies (*10*), which are consistent with some degree of ring stacking. *Ab initio* computer calculations indicate this *endo* transition state is 2−8 kcal/mol more stable than the *exo* conformer (that describes the transition state for chromosomal DHFR) due to interligand interactions (*34*, *35*). Use of a more stable transition state may be one mechanism by which R67 DHFR overcomes the constraints imposed by its 222 symmetry and catalyzes its reaction. Stated in a different way, Figure 4 supports the proposal that interligand interactions are critical for binding, which ultimately leads to formation of an *endo* transition state where the rings of the ligands partially overlap.

A more well-evolved enzyme would not necessarily show this pattern as it may utilize more sophisticated approaches to catalysis. For example, *E. coli* (*Ec*) chromosomal DHFR utilizes an aspartic acid (D27) in its active site to facilitate catalysis (*36*−*42*). In addition, an *exo* transition state is proposed for *Ec* chromosomal DHFR; thus, cooperativity between ligands appears to be less pivotal (*35*). Finally, a role for coupled motion in *Ec* chromosomal DHFR has recently been proposed to funnel energy toward achieving catalysis (*43*−*48*). Thus, these more sophisticated devices would most likely need to be weakened in order to observe a more basic underpinning of catalysis (i.e., a correlation between enthalpy and efficiency) occurring in *E. coli* chromosomal DHFR (*49*).

Our studies also support recent reports suggesting a strong role for enthalpy associated with catalytic function (*50*−*54*). One example of interest involves studies of single mutants for horse liver alcohol dehydrogenase in which the "bulky" active site residue (Val203) was replaced with smaller residues (*55*). A molecular dynamics study of this system indicated a decrease in log $k_{cat}/K_m$ was correlated with an increasing MD-derived contact distance between reactants (*56*). The bulky side chain, therefore, reduced the distance between the reactants, suggesting a correlation between catalytic efficiency and contact distance.

*Conclusion.* The catalytic strategy of R67 DHFR arises from the need to balance efficiency with the symmetry imposed by the structure. This constraint dictates a one site fits both approach to catalysis in which each residue plays a dual role in cofactor and substrate binding. The residues with the largest role have been identified by a mutagenesis strategy and are K32, Q67, I68, and Y69. Q67 and I68 define the center of the hourglass pore, while Y69 and K32 extend this binding surface to the edge of the pore. These residues establish a contiguous stripe that describes the binding

surface. Inextricably coupled to the symmetry is the need to differentiate between nonproductive (two NADPH or two DHF molecules) and productive (NADPH·DHF) complexes. The mechanism by which this is achieved involves interligand cooperativity patterns, where strong positive cooperativity between NADPH and DHF funnels the enzyme toward the ternary complex. This positive cooperativity clearly possesses an enthalpic basis, and Figure 4 extends this linkage to catalytic efficiency.

## REFERENCES


1. Strader, M. B., Smiley, R. D., Stinnett, L. G., VerBerkmoes, N. C., and Howell, E. E. (2001) Role of S65, Q67, I68, and Y69 residues in homotetrameric R67 dihydrofolate reductase, *Biochemistry 40*, 11344−11352.
2. Hicks, S. N., Smiley, R. D., Hamilton, J. B., and Howell, E. E. (2003) Role of ionic interactions in ligand binding and catalysis of R67 dihydrofolate reductase, *Biochemistry 42*, 10569−10578.
3. Park, H., Bradrick, T. D., and Howell, E. E. (1997) A glutamine 67 → histidine mutation in homotetrameric R67 dihydrofolate reductase results in four mutations per single active site pore and causes substantial substrate and cofactor inhibition, *Protein Eng. 10*, 1415−1424.
4. Amyes, S. G., Towner, K. J., and Young, H. K. (1992) Classification of plasmid-encoded dihydrofolate reductases conferring trimethoprim resistance, *J. Med. Microbiol. 36*, 1−3.
5. White, P. A., and Rawlinson, W. D. (2001) Current status of the aadA and dfr gene cassette families, *J. Antimicrob. Chemother. 47*, 495−496.
6. Reece, L. J., Nichols, R., Ogden, R. C., and Howell, E. E. (1991) Construction of a synthetic gene for an R-plasmid-encoded dihydrofolate reductase and studies on the role of the N-terminus in the protein, *Biochemistry 30*, 10895−10904.
7. Narayana, N., Matthews, D. A., Howell, E. E., and Xuong, N. H. (1995) A plasmid-encoded dihydrofolate reductase from trimethoprim-resistant bacteria has a novel D2-symmetric active site, *Nat. Struct. Biol. 2*, 1018−1025.
8. Bradrick, T. D., Beechem, J. M., and Howell, E. E. (1996) Unusual binding stoichiometries and cooperativity are observed during binary and ternary complex formation in the single active pore of R67 dihydrofolate reductase, a D2 symmetric protein, *Biochemistry 35*, 11414−11424.
9. Pitcher, W. H., III, DeRose, E. F., Mueller, G. A., Howell, E. E., and London, R. E. (2003) NMR studies of the interaction of a type II dihydrofolate reductase with pyridine nucleotides reveal unexpected phosphatase and reductase activity, *Biochemistry 42*, 11150−11160.
10. Howell, E. E., Shukla, U., Hicks, S. N., Smiley, R. D., Kuhn, L. A., and Zavodszky, M. I. (2001) One site fits both: a model for the ternary complex of folate + NADPH in R67 dihydrofolate reductase, a D2 symmetric enzyme, *J. Comput.-Aided Mol. Des. 15*, 1035−1052.
11. Li, D., Levy, L. A., Gabel, S. A., Lebetkin, M. S., DeRose, E. F., Wall, M. J., Howell, E. E., and London, R. E. (2001) Interligand Overhauser effects in type II dihydrofolate reductase, *Biochemistry 40*, 4242−4252.
12. Liang, J., Edelsbrunner, H., and Woodward, C. (1998) Anatomy of protein pockets and cavities: measurement of binding site geometry and implications for ligand design, *Protein Sci. 7*, 1884−1897.
13. Howell, E. E., Warren, M. S., Booth, C. L., Villafranca, J. E., and Kraut, J. (1987) Construction of an altered proton donation mechanism in *Escherichia coli* dihydrofolate reductase, *Biochemistry 26*, 8591−8598.
14. Ellis, K. J., and Morrison, J. F. (1982) Buffers of constant ionic strength for studying pH-dependent processes, *Methods Enzymol. 87*, 405−426.
15. Smiley, R. D., Stinnett, L. G., Saxton, A. M., and Howell, E. E. (2002) Breaking symmetry: mutations engineered into R67 dihydrofolate reductase, a D2 symmetric homotetramer possessing a single active site pore, *Biochemistry 41*, 15664−15675.
16. Gornall, A. G., Bardawill, C. J., and David, M. M. (1949) Determination of serum proteins by means of the biuret reaction, *J. Biol. Chem. 177*, 751−766.
17. Blakley, R. L. (1960) Crystalline dihydropteroylglutamic acid, *Nature 188*, 231−232.
18. Horecker, B. L., and Kornberg, A. (1948) The extinction coefficients of the reduced band of pyridine nucleotides, *J. Biol. Chem. 175*, 385−390.
19. Baccanari, D., Phillips, A., Smith, S., Sinski, D., and Burchall, J. (1975) Purification and properties of *Escherichia coli* dihydrofolate reductase, *Biochemistry 14*, 5267−5273.
20. Wiseman, T., Williston, S., Brandts, J. F., and Lin, L. N. (1989) Rapid measurement of binding constants and heats of binding using a new titration calorimeter, *Anal. Biochem. 179*, 131−137.
21. Nichols, R., Weaver, C. D., Eisenstein, E., Blakley, R. L., Appleman, J., Huang, T. H., Huang, F. Y., and Howell, E. E. (1993) Titration of histidine 62 in R67 dihydrofolate reductase is linked to a tetramer ↔ two-dimer equilibrium, *Biochemistry 32*, 1695−1706.
22. Royer, C. A., Mann, C. J., and Matthews, C. R. (1993) Resolution of the fluorescence equilibrium unfolding profile of trp aporepressor using single tryptophan mutants, *Protein Sci. 2*, 1844−1852.
23. West, F. W., Seo, H. S., Bradrick, T. D., and Howell, E. E. (2000) Effects of single-tryptophan mutations on R67 dihydrofolate reductase, *Biochemistry 39*, 3678−3689.
24. Whitman, C. P. (2002) The 4-oxalocrotonate tautomerase family of enzymes: how nature makes new enzymes using a $\beta$-$\alpha$-$\beta$ structural motif, *Arch. Biochem. Biophys. 402*, 1−13.
25. Lovell, S. C., Word, J. M., Richardson, J. S., and Richardson, D. C. (2000) The penultimate rotamer library, *Proteins 40*, 389−408.
26. Park, H., Zhuang, P., Nichols, R., and Howell, E. E. (1997) Mechanistic studies of R67 dihydrofolate reductase. Effects of pH and an H62C mutation, *J. Biol. Chem. 272*, 2252−2258.
27. Calderone, C. T., and Williams, D. H. (2001) An enthalpic component in cooperativity: the relationship between enthalpy, entropy, and noncovalent structure in weak associations, *J. Am. Chem. Soc. 123*, 6262−6267.
28. Williams, D. H., Stephens, E., and Zhou, M. (2003) How can enzymes be so efficient? *Chem. Commun.*, 1973−1976.
29. Williams, D. H., Stephens, E., and Zhou, M. (2003) Ligand binding energy and catalytic efficiency from improved packing within receptors and enzymes, *J. Mol. Biol. 329*, 389−399.
30. Warshel, A. (1998) Electrostatic origin of the catalytic power of enzymes and the role of preorganized active sites, *J. Biol. Chem. 273*, 27035−27038.
31. Warshel, A., Florian, J., Strajbl, M., and Villa, J. (2001) Circe effect versus enzyme preorganization: what can be learned from the structure of the most proficient enzyme? *ChemBioChem 2*, 109−111.
32. Szwajkajzer, D., and Carey, J. (1997) Molecular and biological constraints on ligand-binding affinity and specificity, *Biopolymers 44*, 181−198.
33. Wedemayer, G. J., Patten, P. A., Wang, L. H., Schultz, P. G., and Stevens, R. C. (1997) Structural insights into the evolution of an antibody combining site, *Science 276*, 1665−1669.
34. Andres, J., Moliner, V., Safont, V. S., Domingo, L. R., Picher, M. T., and Krechl, J. (1996) On transition structures for hydride transfer step: a theoretical study of the reaction catalyzed by dihydrofolate reductase enzyme, *Bioorg. Chem. 24*, 10−18.
35. Castillo, R., Andres, J., and Moliner, V. (1999) Catalytic Mechanism of Dihydrofolate Reductase Enzyme. A Combined Quantum-Mechanical/Molecular-Mechanical Characterization of Transition State Structure for the Hydride Transfer Step, *J. Am. Chem. Soc. 121*, 12140−12147.
36. Howell, E. E., Villafranca, J. E., Warren, M. S., Oatley, S. J., and Kraut, J. (1986) Functional role of aspartic acid-27 in dihydrofolate reductase revealed by mutagenesis, *Science 231*, 1123−1128.
37. Chen, Y. Q., Kraut, J., Blakley, R. L., and Callender, R. (1994) Determination by Raman spectroscopy of the pKa of N5 of dihydrofolate bound to dihydrofolate reductase: mechanistic implications, *Biochemistry 33*, 7021−7026.
38. Lee, H., Reyes, V. M., and Kraut, J. (1996) Crystal structures of *Escherichia coli* dihydrofolate reductase complexed with 5-formyltetrahydrofolate (folinic acid) in two space groups: evidence for enolization of pteridine O4, *Biochemistry 35*, 7012−7020.
39. Cannon, W. R., Garrison, B. J., and Benkovic, S. J. (1997) Consideration of the pH-dependent inhibition of dihydrofolate reductase by methotrexate, *J. Mol. Biol. 271*, 656−668.
40. Casarotto, M. G., Basran, J., Badii, R., Sze, K. H., and Roberts, G. C. (1999) Direct measurement of the p$K_a$ of aspartic acid 26

in *Lactobacillus casei* dihydrofolate reductase: implications for the catalytic mechanism, *Biochemistry 38*, 8038−8044.
41. Rod, T. H., and Brooks, C. L., III (2003) How dihydrofolate reductase facilitates protonation of dihydrofolate, *J. Am. Chem. Soc. 125*, 8718−8719.
42. Rod, T. H., Radkiewicz, J. L., and Brooks, C. L., III (2003) Correlated motion and the effect of distal mutations in dihydrofolate reductase, *Proc. Natl. Acad. Sci. U.S.A. 100*, 6980−6985.
43. Rajagopalan, P. T., Lutz, S., and Benkovic, S. J. (2002) Coupling interactions of distal residues enhance dihydrofolate reductase catalysis: mutational effects on hydride transfer rates, *Biochemistry 41*, 12618−12628.
44. Rajagopalan, P. T., and Benkovic, S. J. (2002) Preorganization and protein dynamics in enzyme catalysis, *Chem. Rec. 2*, 24−36.
45. Radkiewicz, J., and Brooks, I. C. (2000) Protein Dynamics in Enzymatic Catalysis: Exploration of Dihydrofolate Reductase, *J. Am. Chem. Soc. 122*, 225−231.
46. Agarwal, P. K., Billeter, S. R., Rajagopalan, P. T., Benkovic, S. J., and Hammes-Schiffer, S. (2002) Network of coupled promoting motions in enzyme catalysis, *Proc. Natl. Acad. Sci. U.S.A. 99*, 2794−2799.
47. Agarwal, P. K., Billeter, S. R., and Hammes-Schiffer, S. (2002) Nuclear quantum effects and enzyme dynamics in dihydrofolate reductase catalysis, *J. Phys. Chem. B 106*, 3283−3293.
48. Benkovic, S. J., and Hammes-Schiffer, S. (2003) A perspective on enzyme catalysis, *Science 301*, 1196−1202.
49. Kraut, D. A., Carroll, K. S., and Herschlag, D. (2003) Challenges in enzyme mechanism and energetics, *Annu. Rev. Biochem. 72*, 517−571.
50. Bruice, T. C. (2002) A view at the millennium: the efficiency of enzymatic catalysis, *Acc. Chem. Res. 35*, 139−148.
51. Bruice, T. C., and Benkovic, S. J. (2000) Chemical basis for enzyme catalysis, *Biochemistry 39*, 6267−6274.
52. Bruice, T. C., and Lightstone, F. C. (1999) Ground State and Transition State Contributions to the Rate of Intramolecular and Enzymic Reactions, *Acc. Chem. Res. 32*, 127−136.
53. Wolfenden, R., and Snider, M. J. (2001) Ground State and Transition State Contributions to the Rate of Intramolecular and Enzymic Reactions, *Acc. Chem. Res. 34*, 938−945.
54. Wolfenden, R., Snider, M., Ridgway, C., and Miller, B. (1999) The Temperature Dependence of Enzyme Rate Enhancements, *J. Am. Chem. Soc. 121*, 7419−7420.
55. Bahnson, B. J., Park, D. H., Kim, K., Plapp, B. V., and Klinman, J. P. (1993) Unmasking of hydrogen tunneling in the horse liver alcohol dehydrogenase reaction by site-directed mutagenesis, *Biochemistry 32*, 5503−5507.
56. Luo, J., Kahn, K., and Bruice, T. C. (1999) The linear dependence of $\log(k_{cat}/K_m)$ for reduction of $NAD^+$ by $PhCH_2OH$ on the distance between reactants when catalyzed by horse liver alcohol dehydrogenase and 203 single point mutants, *Bioorg. Chem. 27*, 289−296.
57. Brito, R. M., Reddick, R., Bennett, G. N., Rudolph, F. B., and Rosevear, P. R. (1990) Characterization and stereochemistry of cofactor oxidation by a type II dihydrofolate reductase, *Biochemistry 29*, 9825−9831.
58. Brito, R. M., Rudolph, F. B., and Rosevear, P. R. (1991) Conformation of $NADP^+$ bound to a type II dihydrofolate reductase, *Biochemistry 30*, 1461−1469.

BI049646K